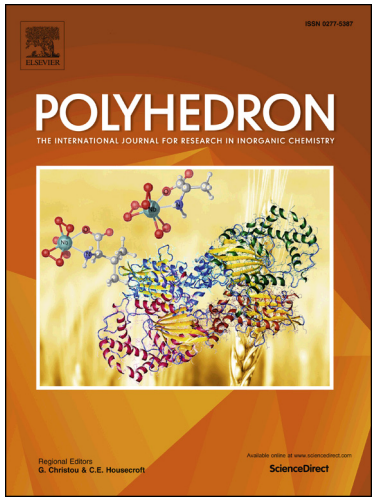

Investigation of Mono-, Bis- and Tris-glycinatochromium(III): Comparisons of Computational and Experimental Results

Kabir M. Uddin, Raymond A. Poirier, David J. Henry

PII: S0277-5387(17)30270-X
DOI: http://dx.doi.org/10.1016/j.poly.2017.04.003
Reference: POLY 12579

To appear in: *Polyhedron*

Received Date: 13 February 2017
Revised Date: 3 April 2017
Accepted Date: 4 April 2017

Please cite this article as: K.M. Uddin, R.A. Poirier, D.J. Henry, Investigation of Mono-, Bis- and Tris-glycinatochromium(III): Comparisons of Computational and Experimental Results, *Polyhedron* (2017), doi: http://dx.doi.org/10.1016/j.poly.2017.04.003

Investigation of Mono-, Bis- and Tris-glycinatochromium(III): Comparisons of Computational and Experimental Results

Kabir M. Uddin,[‡] Raymond A. Poirier[§] and

David J. Henry*[,‡]

[‡]Chemical and Metallurgical Engineering and Chemistry,
Murdoch University, Western Australia, 6150
Australia

[§]Department of Chemistry, Memorial University,
St. John's, Newfoundland,
Canada A1B 3X7

Tel.: (08) 9360-2681
E-mail: d.henry@murdoch.edu.au

Abstract:

The synthesis and characterization of mono-, bis- and tris-glycinatochromium(III) complexes by UV-Vis, electron paramagnetic resonance (EPR), ATR-FTIR and Raman spectroscopy has been performed in this work. IR stretching bands obtained from DFT calculations of the mono-, bis- and tris-glycinatochromium(III) complexes are in good agreement with experimental data. Different mechanistic pathways were explored for the water exchange reactions of $[Cr(^{+}NH_3CH_2COO^{-})(H_2O)_5]^{3+}$ and its conjugate base species including, associative interchange (I_a), and dissociative (D) mechanisms. The lowest activation enthalpies for the mono- and bis-complexes are obtained for the I_a pathways with explicit outer sphere solvation (88 and 76 kJ mol^{-1}), which are in good agreement with the experimental values (87 and 75 kJ mol^{-1}). In comparison, tris-glycinatochromium(III) undergoes aquation via the dissociative (D) mechanism. Investigation of these systems in the pH range ~3.0 to ~8.5 by UV-Vis monitoring, helps identify the speciation of these complexes in physiological environments.

Keywords: Mono-, bis- and tris-glycinatochromium(III) complexes, EPR, UV-Vis, ATR-FTIR, Raman, DFT.

1. Introduction

Chromium(III)–amino acid (AA) complexes are commonly found in nutritional supplements and their physiological activity is of biological importance [1–6]. Several studies [7–10] suggest that Cr(III) in nutritional supplements is of minimal benefit to the function of healthy biological systems. However, there has been significant evidence showing that daily treatment of alloxan-induced diabetic (AID) mice with 500 and 1000 μg Cr/kg body weight (BW) of a Cr(III)–AA complex such as chromium methionine (CrMet) [10], has significant beneficial effects as an insulin enhancing treatment and is more effective than chromium trichloride hexahydrate ($CrCl_3.6H_2O$) and chromium nicotinate (CrNic). There are also reports suggesting that CrMet has a beneficial impact on body weight, triglyceride, total cholesterol and liver glycogen levels, while also reducing lipid metabolism [10]. However, the details of the bio-inorganic pathways for these complexes are not known. Trivalent chromium complexes administered orally will encounter a number of different physiological environments (pH and chemical conditions) as they pass through the body including the high acidity of the stomach and the slightly alkaline conditions of the bloodstream. These differing conditions provide opportunities for chromium(III) complexes to undergo ligand substitution. Furthermore, olation and precipitation can occur at neutral or alkaline pH. It also appears that the bioinorganic mechanism depends upon the ligands coordinated to chromium, with a very slow rate of exchange with the active sites of enzymes [1–2].

It is well-known that the amino acids (AA) can adopt several forms including anion (AA^-), zwitterion (HAA), or cation (H_2AA^+) (see Fig. 1a) depending on the pH of the solution.

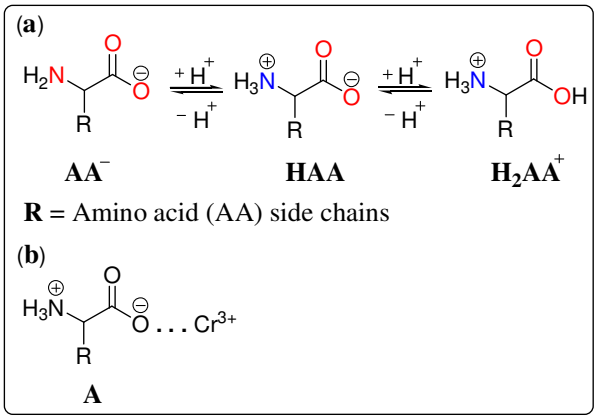

Fig. 1. (a) Protolytic forms of glycine and amino acids (R is the amino acid side chain) and (b) Cr(III) metal interaction with the amino acid zwitterion to form monodentate Cr(III) complex (**A**).

Characterization studies suggests that coordination of Cr(III) with amino acid ligands (e.g. glycine, serine and methionine) occurs through the glycinate nitrogen and carboxylate oxygen to form a chelate ring. However, side chain functional groups can also play a prominent role in metal ion binding at physiological pH. There have been a number of experimental investigations of Cr(III)-AA complexes [11–18]. For example, Abdullah et al. [12] measured the kinetics for the formation of tetra-aquaglycinechromium(III) (pH = 3.0–3.8, temperature = 40–45 °C and ionic strength = 0.4 mol dm^{-3}). They proposed an associative interchange (I_a) pathway with outer-sphere complexation involving glycine-hexa-aquachromium(III) ($\Delta H^{\ddagger}$ = 87 kJ mol^{-1}) or its conjugate base ($\Delta H^{\ddagger}$ = 75 kJ mol^{-1}) [12]. By contrast, the dissociative mechanism has been reported for reaction of $[Cr(NH_3)_5(H_2O)]^{3+}$ with glycine ($\Delta H^{\ddagger}$ = 106 kJ mol^{-1} and $\Delta S^{\ddagger}$ = +23.5 J $mol^{-1}K^{-1}$) [13]. In the pH range 3.0 to 4.5, chromium(III) will interact with amino acids in the zwitterion (HAA) and cationic (H_2AA^+) forms [11–12,16]. Therefore, the formation of the chromium(III)–AA complex (**A**) is coupled with the acid dissociation equilibrium of the amino acid as shown in Fig. 1b.

Cr(III) can coordinate up to 3 glycinate ligands to give the mono-, bis-, and tris-glycinatochromium(III) species. In addition to formation studies, there have been several experimental aquation studies of Cr(III)-AA complexes [17–22]. Kita et al. [23] obtained $\Delta H^{\ddagger}$ and $\Delta S^{\ddagger}$ values of 91.4 ± 2 kJ mol^{-1} and 17 ± 7 J mol^{-1} K^{-1} for acid-catalysed and 66.7 ± 16 kJ mol^{-1} and −71 ± 53 J mol^{-1} K^{-1} for base-catalysed aquation of $[Cr(gly)_3]$. There is evidence that the acid-catalysed aquation of *fac*-$[Cr(gly)_3]^0$ is initiated by dissociation of the Cr–N bond [23]. They also determined that $[Cr(gly)_2(OH)_2]^-$ undergoes base-catalysed aquation ~4 times faster than $[Cr(gly)_2(O–gly)(OH)]^-$. Furthermore, Kita and Lisiak reported [24] that the acid-catalysed aquation of the $[Cr(ox)_2(AA)]^{2-}$ complexes (where AA = alanine (Ala^-), valine (Val^-) or cysteine (Cys^-)) involves formation of a metastable intermediate with a monodentate O-bonded ligand. Kiersikowska et al. also investigated [25–26] the acid- and base-catalysed aquation of *fac*-$[Cr(Aa)_3]$ (Aa = Gly, Ala, Asn) and its aqua derivatives. However, to date there have not been any theoretical studies of the intimate details of ligand exchange on Cr(III)-AA complexes.

Recently we reported [27–29] theoretical studies of aquation of chromium(III) chloride and other dihalides under acidic conditions, as might be found in the stomach after oral ingestion of these species. A key finding in these studies was the importance of outer-sphere solvation on the reaction mechanism. We have also studied [29] the aquation of conjugate-base systems of chromium(III), which is favourable under physiological conditions (pH ~ 7.4), where once again outer sphere solvation is involved in the reaction mechanism. Therefore, the study of these systems leads to a better understanding of the stability and speciation under physiological conditions, prior to binding to enzymes or peptides. Investigation of the aquation of mono-, bis-,

and tris-glycinatochromium(III) complexes may also provide insight into the stability of chromium(III) protein complexes. Recently, Uddin et al. [30] studied the synthesis of the *fac*-[$Cr(gly)_3$] complex, which was fully characterized by elemental analysis, AAS, ESI-mass spectrometry, UV-Vis, EPR and ^{1}H NMR spectroscopy. Furthermore, the electrochemical properties of *fac*-[$Cr(gly)_3$] were investigated by cyclic voltammetry and the thermal decomposition determined using differential scanning calorimetry (DSC).

To date, no computational mechanistic studies have been reported for the aquation of open-type monodentate and closed-type bidentate systems of glycinato-chromium(III) ($[Cr(gly)_x(H_2O)_{6-2x}]^{(3-x)+}$ where x = 1 –3) and their conjugate bases species. Therefore, the major objective of this study is to provide a detailed investigation of the pathways for these processes using DFT calculations. Theoretical calculations are complemented by experimental characterisation of $[Cr(gly)(H_2O)_4]Cl_2$, $[Cr(gly)_2(H_2O)]Cl$, and $[Cr(gly)_3]$ by elemental analysis, thermal analysis, UV−Vis, EPR, ATR-IR, and Raman spectroscopy.

2. Experimental

2.1. Reagents

Chromium(III) chloride hexahydrate, $CrCl_3.6H_2O$ (Sigma-Aldrich, ≥98.0%), glycine (Sigma-Aldrich, ≥98.5%), ethanol (LabServ, 99.8%) and sodium hydroxide (Sigma-Aldrich, 98.5%) were used without further purification. Millipore filtered deionized water was used throughout the experimental work.

2.2. Analytical Methods

Elemental analysis (C, H, and N) was performed using the microanalytical unit, J Science lab JM 11 analyzer. Determination of Cr was carried out using atomic absorption spectroscopy (a

Varian AA50 spectrometer with air/C_2H_2 flame atomization) after digestion of the samples with 69% HNO_3 (Merck). Chloride present in the complexes was assessed by Volhard's method. Thermal analysis was conducted using a PerkinElmer STA 8000 TGA-DSC instrument. Before the heating routine program was activated, the entire system was purged with argon for 10 min at a rate of 20 mL/min, to ensure that the desired environment was established. Thermogravimetric analysis (TGA) experiments were performed with a heating rate of 20 °C min^{-1} from 30 to 1000 °C. High-purity argon gas was used at a constant flow rate of 20 mL/min. Solution ultraviolet-visible (UV-Vis) spectra were recorded on a HP 8453 UV-Vis spectrophotometer over the range 190−1100 nm. A Bruker EMX EPR spectrometer running the Xenon software with a Bruker ER 036TM NMR tesla meter was used to measure the X-band spectra of the solid Cr(III) complexes with EP parameters: center field, 3200 G; sweep width, 6000 G; width TM, 200 G; Frequency Mon, 9.79 GHz; microwave power, 2.0 mW; microwave attenuation, 20.0 dB; conversion time, 4.0 ms; gain, 30dB; modulation amplitude, 4.0 G; modulation frequency, 100 kHz; resolution, 15000 and sweep time, 60 s. For frozen solution samples, the EPR tube was flushed with with nitrogen gas for 2 min before analysis and the samples frozen by slow immersion in a liquid nitrogen bath. EPR parameters for frozen samples were gain, 1.0×10^4; modulation frequency, 100 kHz; modulation amplitude, 1 G; conversion time, 0.41 ms; time constant, 81.92 ms; sweep time, 41.98 s; field center, 3350 G; sweep width, 6400 G; frequency, 9.531415 GHz; and power, 2.0 mW.

Infrared analysis was carried out using a Perkin Elmer FT-IR with a universal ATR sampling accessory. ATR spectra were generated using 4 scans with a resolution of 4 cm^{-1} in a range of 4000−350 cm^{-1}. A constant pressure between the ATR foot, sample and ATR crystal was achieved using an in-built pressure gauge and software monitor. Raman analysis was conducted

using a Nicolet 6700 FT-IR with NXR FT-Raman module. Raman spectra were collected with: 1064 nm excitation wavelength, 90^{o} detection angle, CaF_2 beam splitter, InGaAs detector, gain of 1, optical velocity of 0.3165, aperture of 150, focus and side-to-side settings optimised, laser power of 1.5 W and 256 scans with resolution of 8 cm^{-1} in the range 4000−200 cm^{-1}.

The pH of solutions was measured using LabCHEM-pH meter with a PBFB electrode and calibration of the pH combination electrode was carried out.

2.3. Preparation of $[Cr(gly)(H_2O)_4]Cl_2$ and $[Cr(gly)_2(H_2O)_2]Cl$

The *fac*-$[Cr(gly)_3]$ complex was synthesized and fully characterized as reported previously [30]. The mono- and bis-glycinatochromium(III) chloride complexes were synthesised in the current study using 1:1 and 1:2 ratios of Chromium(III) chloride hexahydrate, $CrCl_3.6H_2O$ and glycine, prepared according to a similar method used for the tris-system [19,30]. The solid product was collected by vacuum filtration, washed with ethanol and dried at 100°C in an oven. A greenish (light blue) product was obtained for mono-glycinatochromium(III) chloride and a red (light pink) solid was isolated for bis-glycinatochromium(III) chloride. The yield of the reactions were 1.35 g (57%) for mono- and 1.37 g (69%) for bis-dentate chromium(III) glycinate complexes. These complexes were characterised by thermogravimetry, UV-Vis, ATR-FTIR, Raman, and EPR spectroscopy in the solid state (room temp.) and frozen solution state (100 K). Anal. Calcd for $C_2H_{12}Cl_2CrNO_6$: C, 8.93; H, 4.50; Cl, 26.36; N, 5.21; Cr, 19.33. Found: C, 8.91; H, 4.93; Cl, 26.43; N, 4.85; Cr, 18.87. Anal. Calcd for $C_4H_{12}ClCrN_2O_6$: C, 17.69; H, 4.45; Cl, 13.06; N, 10.31; Cr, 19.15. Found: C, 16.67; H, 4.46; Cl, 12.97; N, 10.28; Cr, 18.71.

2.4. Computational Methods

Standard hybrid density functional theory calculations were carried out with Gaussian 09 [31]. The geometries of all complexes in this study were fully optimized in the gas phase and solvent (water) at the PBE0/cc-pVDZ level of theory, which we have previously shown to give excellent agreement with experiment for the activation enthalpies for aquation of related species [27–29]. The effect of solvent (water) on the structures and energetics of each complex was investigated using the polarisable continuum model (PCM) of Tomasi and co-workers [32–33]. Vibrational frequencies were obtained for all optimized structures to check for the absence of imaginary frequencies for reactants, intermediates and products and for the presence of a single imaginary frequency for each transition state. For all the reaction pathways discussed in this study, the transition states were also analyzed using the intrinsic reaction coordinate (IRC) method. The final structures obtained from each IRC were further optimized in order to positively identify the reactant and product complexes to which each transition state is connected.

Natural bonding orbital (NBO) [34] analysis was performed and the charges were calculated. The HOMO and LUMO energies were determined from the ground state quartet geometries. Enthalpies of activation and entropies of activation were calculated at 298.15 K. In the figures, all distances are in angstroms (Å), angles in degrees (º) and the energies in kJ mol^{-1}. Unless otherwise stated, all values given in the text were obtained at the PBE0/cc-pVDZ level in solution (PCM). The optimized structures and the relative energies of reactants, intermediates, transition states, and products for all pathways are shown in Tables ST1 to ST7 and Figs. S1 to S49 of the Supporting Information (SI). The volume of activation ($\Delta V^{\ddagger}$) and reaction volume (ΔV) were correlated to the change in the Cr–L bond lengths of the TS, reactant and product as reported previously [27–29].

The $[Cr(gly)_3]^0$ complex can occur as either a facial or meridional isomer. The XRD crystal structure for $[Cr(gly)_3]^0$ reported by Bryan et al. [19] shows only the facial isomer, which implies that this isomer is the most stable in the solid state. However, our DFT calculations of the complex with PCM solvation indicate that the energies of the *fac*- (I) and *mer*- (II) isomers are almost identical with the meridional structure very slightly favoured (~ 0.5 kJ mol^{-1}) at PBE0/cc-pVDZ (Fig. 2). There have been some reports that suggest that glycine can also form chelate rings via coordination of the two carboxylate oxygen atoms. Therefore, for completeness the stability of two additional structures of the form $[Cr(gly)_2(O_2CCH_2NH_2)]$ (III and IV) were investigated and found to be less energetically stable than those with facial configuration by 30 and 40 kJ mol^{-1}.

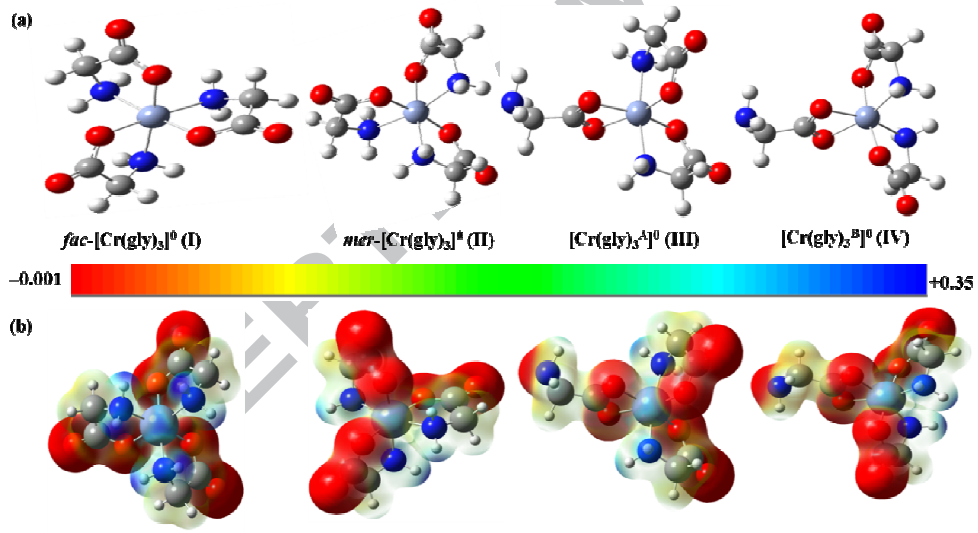

Fig. 2. (a) Optimized structures of the conformers for $[Cr(gly)]_3$ at PBE0/cc-pVDZ; (b) maps of electrostatic potential (0.02 electrons $Bohr^{-3}$) (red = electron-rich, blue = electron-deficient).

As reported recently [30], the calculated Cr–N and Cr–O bond distances for *fac*-$[Cr(gly)_3]$ are in good agreement with the experimental X-ray crystal data [19]. The calculated average values for

the Cr–N and Cr–O bond lengths of *mer*-[Cr(gly)$_3$] are 2.107 and 1.944 Å, respectively (Table ST1 of the SI).

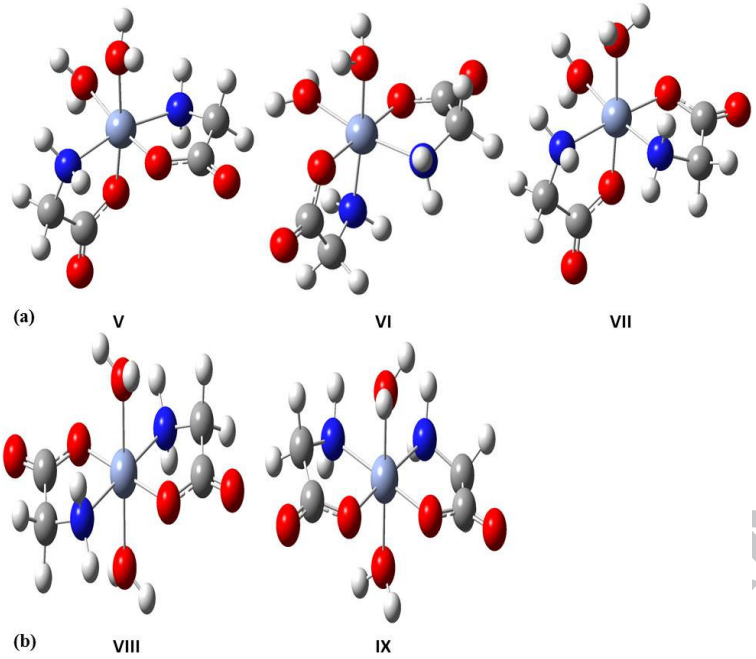

Fig. 3. Optimized conformations of precursor $[Cr(gly)_2(H_2O)_2]^+$ for (a) *cis*-conformers (V–VII forms) and (b) *trans*-conformers (VIII–IX forms) at PBE0/cc-pVDZ.

Three different *cis*-conformations of $[Cr(gly)_2(H_2O)_2]^+$ were investigated with structure (V) the most stable (Fig. 3). Isomers, VI and VII were higher in energy by 1.5 and 6.3 kJ mol^{-1}, respectively. Two *trans* isomers of $[Cr(gly)_2(H_2O)_2]^+$ (VIII and IX) were also investigated and were found to be 4.1 and 19.1 kJ mol^{-1} higher in energy than (V). Isomers of the mono-glycinatochromium(III) complex were also investigated including closed-type bi-dentate (X) and open-type mono-dentate via intramolecular Cr–N ring opening (Fig. 4).

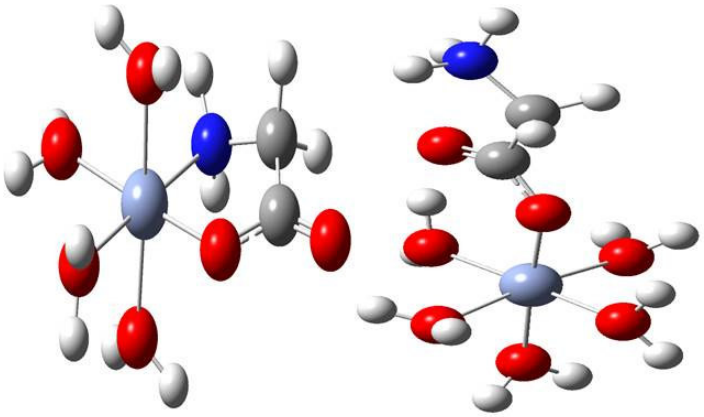

Fig. 4. Optimized structures of $[Cr(gly)(H_2O)_4]^{2+}$ and $[Cr(^{+}NH_3CH_2COO^{-})(H_2O)_5]^{3+}$ at PBE0/cc-pVDZ.

3. Results and Discussion

3.1. Synthesis and characterization of $[Cr(gly)(H_2O)_4]Cl_2$, $[Cr(gly)_2(H_2O)_2]Cl$ and $[Cr(gly)_3]^0$

Mono- and bis-glycinatochromium(III) chloride complexes were synthesized using a similar procedure to that reported previously for $[Cr(gly)_3]^0$ [30]. Elemental analysis (% C, H, Cl, N, and Cr) data confirm the formation of mono- and bis-glycinatochromium(III) chloride complexes. Previously, elemental analysis (% C, H, N, and Cr) and electrospray mass spectrometry (ESI-MS) data confirm the formation of the $[Cr(gly)_3]$ complex [30]. In our earlier work [30], the solid-state UV-Vis spectrum of the synthesised *fac*-$[Cr((gly)_3]^0$ complex revealed two spin-allowed d–d transitions with absorption bands at 388 nm and 510 nm. However, several studies have shown that the absorption spectra of Cr(III) complexes can have significant solvent and pH dependence. For example, Emerson and Graven [35] measured the UV/Vis spectra of chromium(III) perchlorate solutions within a pH range of 2–5 and noted a transition in the absorbance, corresponding to the conversion of the chromium(III) perchlorate solution to

$[Cr(H_2O)_5OH]^{2+}$ [36]. Consequently they were able to report the equilibrium constant for the acid dissociation reaction of $[Cr(H_2O)_6]^{3+}$ to $[Cr(H_2O)_5OH]^{2+}$. Therefore the solvent dependence of UV/Vis spectra of the complexes in this study ($CrCl_3.6H_2O$ (or $[Cr(H_2O)_4Cl_2]^+$), $[Cr(gly)(H_2O)_4]Cl_2$, $[Cr(gly)_2(H_2O)_2]Cl$, and *fac*-$[Cr(gly)_3]^0$) was investigated. The two major spin-allowed d-d bands for the chromium(III) chloride $[Cr(H_2O)_4Cl_2]^+$ starting material were observed at 443 nm (20.6 M^{-1} cm^{-1}) and 634 nm (21.0 M^{-1} cm^{-1}) in water at pH 3.86 (Figs. 5a and S1 to S2 of the SI). Previously, Elving and Zemel examined, $[Cr(H_2O)_4Cl_2]^+$ in 12 M HCl, reporting bands at 450 nm (27.9 M^{-1} cm^{-1}) and 635 nm (23.9 M^{-1} cm^{-1}) [37].

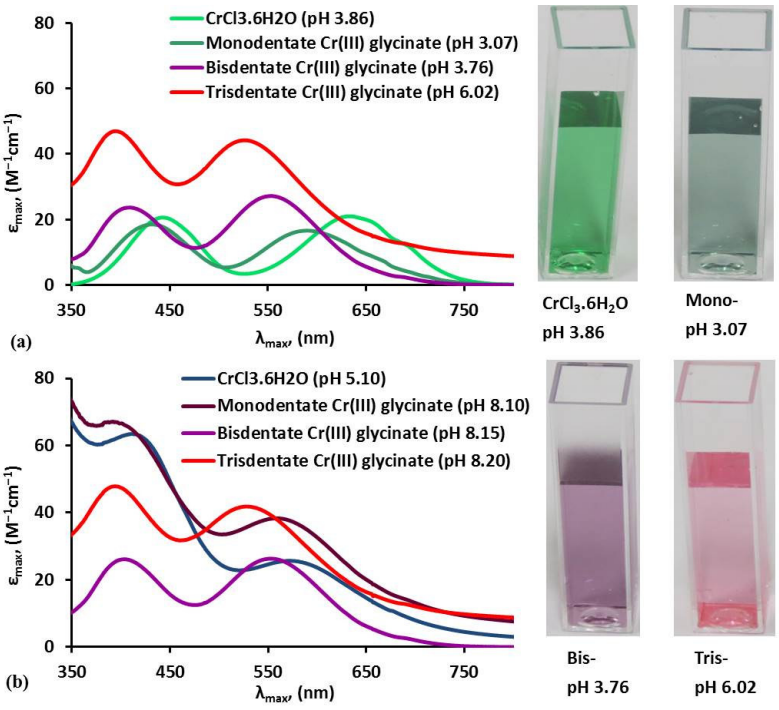

Fig. 5. UV-visible (UV-Vis) spectrum of $CrCl_3.6H_2O$, $[Cr(gly)(H_2O)_4]Cl_2$, $[Cr(gly)_2(H_2O)_2]Cl$ and *fac*-$[Cr(gly)_3]^0$ in the range 350–800 nm at pH ~3.0 to ~8.3, in water. The concentration of the species are c = 11, 21, 14, and 9 mM, respectively.

During formation of mono-glycinatochromium(III) complex at pH 3.07, these two main bands are observed to shift to 433 nm (18.5 M^{-1} cm^{-1}) and 591 nm (16.6 M^{-1} cm^{-1}), respectively (Fig. 5). With the addition of a second glycine ligand to form bis-glycinatochromium(III) at pH 3.76,

there is a further shift of the bands to 409 nm (23.6 M^{-1} cm^{-1}) and 553 nm (27.2 M^{-1} cm^{-1}). Finally, the two bands are located at 395 nm (23.6 M^{-1} cm^{-1}) and 527 nm (44.2 M^{-1} cm^{-1}) for tris-glycinatochromium(III) at pH 6.02 (Fig. 5). Bryan et al. [19] reported the solid UV/Vis spectrum of *fac*-$[Cr(gly)_3]^0$ and assigned $^4A_{2g} \rightarrow {}^4T_{2g}$ to the 503 nm transition and $^4A_{2g} \rightarrow {}^4T_{1g}$ (F) to the 384 nm transition. On this basis, the longer wavelength peaks above can be tentatively attributed to the $^4A_{2g} \rightarrow {}^4T_{2g}$ transition and the shorter wavelength peaks to the $^4A_{2g} \rightarrow {}^4T_{1g}$ (F) transition in the octahedral (O_h) approximation. Mono- and bis-glycinatochromium(III) complexes are intermediates in both the step-wise formation and aquation of tris-glycinatochromium(III) [38−39]. Therefore, the progress of these reactions can be monitored by shifts in these two peaks. As noted above, raising the pH of solutions of chromium(III) species can lead to the formation of the corresponding conjugate base species, which also leads to changes in the absorption spectra. UV-Vis absorption spectra of solutions of $CrCl_3.6H_2O$, $[Cr(gly)(H_2O)_4]Cl_2$, $[Cr(gly)_2(H_2O)_2]Cl$, and *fac*-$[Cr(gly)_3]^0$ at elevated pH are shown in Fig. 5b. Notably, when the pH of $CrCl_3.6H_2O$ and $[Cr(gly)(H_2O)_4]Cl_2$ solutions was raised to ~ 8.1, the samples became cloudy and turned purple indicating the formation of the corresponding conjugate base complexes and subsequent formation of oligomeric species. However, $[Cr(gly)_2(H_2O)_2]Cl$ and *fac*-$[Cr(gly)_3]^0$ complexes were less susceptible to this change in pH and gave identical spectra under acidic and alkaline conditions as shown in Fig. 5b. The aqueous deprotonation of $[Cr(gly)_x(H_2O)_{6-2x}]^{(3-x)+}$ (where x = 1 – 3), and their conjugate bases was investigated by DFT using reactions of the following form:

$$[Cr(H_2O)_5(OglyH)]^{3+} \leftrightarrows [Cr(H_2O)_4(gly)]^{2+} + H_3O^+ \quad (1)$$

$$[Cr(H_2O)_4(gly)]^{2+} + H_2O \leftrightarrows [Cr(H_2O)_4(OH)(gly)]^{+} + H_3O^+ \quad (2)$$

Consequently, we have calculated aqueous Gibbs free energies for deprotonation (ΔG_{dp}) using reactions (1) and (2), for the mono-, bis-, and tris-species. The ΔG_{dp} values decrease for these two reactions from tris- through to the mono-species (see Figs. S2A–S2B in the SI), with a variation of ~ 35 and ~ 111 kJ mol^{-1} , respectively, across the series. The large positive ΔG_{dp} values for the tris- and bis-species indicates that deprotonation of these complexes is not favourable and corresponds with the experimentally observed inertness towards mildly alkaline conditions. The lower calculated ΔG_{dp} for mono-glycinatochromium(III) represents a greater propensity for formation of the corresponding conjugate base species and is consistent with the experimentally observed colour change and precipitate formation.

Thermogravimetric (TG) analysis under argon was carried out to determine the stability of the mono- and bis-glycinatochromium(III) chloride complexes (Figs. 6a and S3 in the SI). In this work, the differential scanning calorimetry (DSC) curves show three endothermic stages of mass loss in the temperature ranges (a) (50 °C to 280 °C), (b) (350 °C to 480 °C), and (c) (750 °C to 920 °C) for mono- and bis- complexes with a heating rate of 20 °C min^{-1} from 30 to 1000 °C. The first stage shows a gradual weight loss indicating the release of lattice water for both mono- and bis- complexes. A second mass loss occurs around 383 °C for mono-, 413 °C for bis- and 424 °C for tris-glycinatochromium(III) [30] (Fig. 6a) corresponding to the decomposition of the glycine ligand(s). Notably, the transition temperature increases across the series from mono, bis and tris-glycinato complexes, reflecting the increased stability with increased chelation. However, these transition temperatures are lower than the value recently reported by Freitas et al. [40] (472 °C) for tris(8-hydroxyquinolinate)chromium(III).

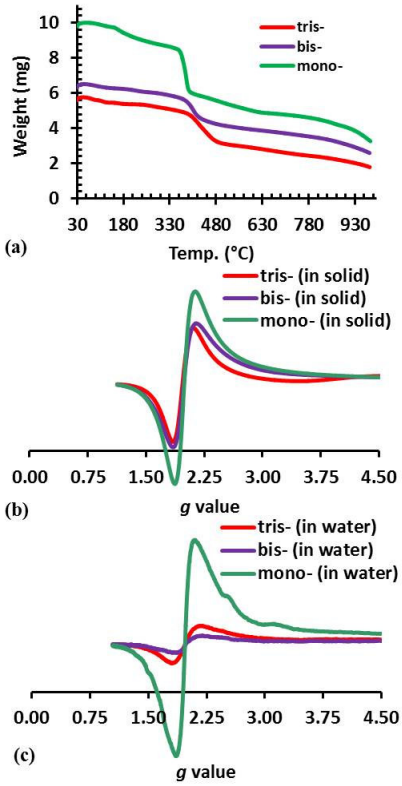

Fig. 6. (a) Thermogravimetric (TG) analysis and analysis of X-band EPR spectra for tris-, bis- and mono-glycinatochromium(III) species, (b) in solid state (room temp.), (c) in frozen state (100 K) and 15.3 mM (red), 14.4 mM (violet) and 20.9 mM (dark blue) in H_2O, respectively.

The paramagnetic behaviour of these octahedral chromium(III) complexes should be sensitive to these changes in coordination environment and can be characterized by two different X-band EPR signals. The g = ~2 β–signal is a broad isotropic signal and the g = 3.5–5.5 δ–signal is a positive lobe in the region [41–43]. In this study, the broad β–signal of the solid EPR gradually decreases from 1.9924 to 1.9886 for mono-, bis-, and tris-glycinatochromium(III) complexes, respectively, (Fig. 6b). For the mono-, bis-, and tris-glycinatochromium(III) series of complexes, the Cr(III) coordination environment changes from $(CO_2)(NH_2)(H_2O)_4$ to $(CO_2)_2(NH_2)_2(H_2O)_2$ to $(CO_2)_3(NH_2)_3$, respectively. Values obtained in the frozen solution state at 100 K in H_2O are slightly lower (g = 1.9710, 1.9737, and 1.9787 [30], for mono-, bis- and tris-

glycinatochromium(III) species, respectively) (see Fig. 6c), which may be the result of solvent effects [30,43].

3.2. Vibrational Spectra of $[Cr(gly)_3]^0$,$[Cr(gly)_2(H_2O)_2]Cl$ and $[Cr(gly)(H_2O)_4]Cl_2$

The IR and Raman spectra of solid glycine, tris-, bis-, and mono-glycinatochromium(III) complexes are presented in Fig. 7 (see Figs. S4–S13 and Table ST2 of the SI). These spectra indicate that glycine coordinates to Cr(III) in the mono-, bis-, and tris-systems via the carboxylate and amino groups (see Fig. S4 of the SI). For example, the $[Cr(gly)_3]^0$ complex has six IR(Raman) frequencies attributed to NH_2 motions including, asymmetric (~3222 (~3248) cm^{-1}) and symmetric (~3134 (~3184) cm^{-1}) N–H stretches, and the NH_2 scissoring (~1590 (~1593) cm^{-1}), twisting (~1311 (~1325) cm^{-1}), wagging (~1144 (~1161) cm^{-1}) and rocking (~752 (~746) cm^{-1}) vibrations (Figs. 7 and S4–S5 and Table S1). Furthermore, the $-COO^-$ stretching bands of the free glycine acid, ν(C=O) = 1586 (1564) cm^{-1} and ν(C–O) = 1412 (1410) cm^{-1}, are transformed in the complexes via $\nu_{as}(COO^-)$ and $\nu_s(COO^-)$ stretching vibrations of the carboxylate group. In the spectrum of $[Cr(gly)_3]^0$ the antisymmetric COO^- vibrations appeared in the range 1690–1630 (1658–1629) cm^{-1}, whereas the symmetric COO^- vibrations for the C–O stretching bands are in the range 1425–1379 (1430–1405) cm^{-1} (Fig. 7 and Table S1). As can be seen from these ranges, the variance between the $\nu_{as}(COO^-)$ and $\nu_s(COO^-)$ stretching vibrations of the carboxylate group is larger than 200 cm^{-1}. Generally, differences of this magnitude between $\nu_{as}(COO^-)$ and $\nu_s(COO^-)$ are attributed to resonance, which arises when the carboxylate group is deprotonated or coordinated to a metal [44–46]. Guindy et al. [14] reported the IR spectrum of solid $Cr(leu)_2$, which showed a shift of the carboxyl group ($\Delta_\nu = \nu_{as} - \nu_s$) of 254

cm^{-1}. Likewise for solid CrMet, the observed [9] difference is 219 cm^{-1}. There is reasonable agreement between the experimental and theoretical data (Table ST2 and Figs. S4–S13 of the SI), for all three complexes.

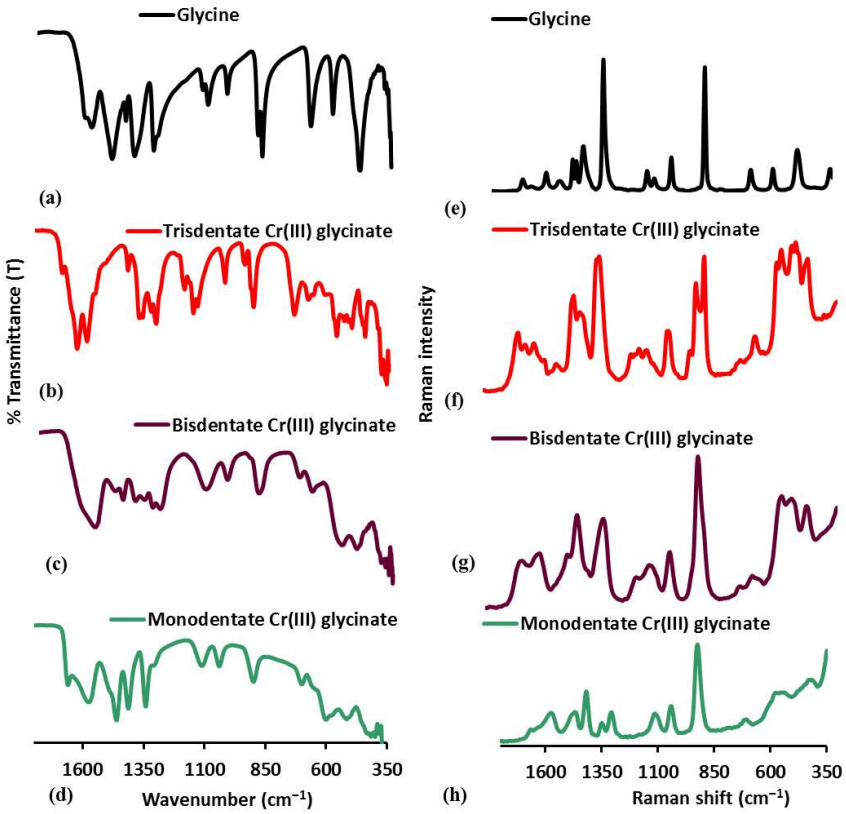

Fig. 7. ATR-IR (a–d) and Raman (e–h) spectra (1800–350 cm^{-1}) for glycine tris-, bis-, and mono-glycinatochromium(III) complexes.

In the spectrum of tris-, bis-, and mono-glycinatochromium(III) complexes, the C–N stretching bands are observed at 1032 (1043), 1038 (1040) and 1039 (1041) cm^{-1}, respectively, whereas the free glycine band was observed at 1033 (1036) cm^{-1} (see Table ST2). The C–C–N bending vibration of glycine with Cr(III) metal is assigned to the bands at 917 (894), 912 (923) and 898 (924) cm^{-1} for tris-, bis-, and mono-glycinatochromium(III) species, respectively, whereas in the free glycine the band appears at 924 (893) cm^{-1} (Fig. 7). The O–C–O wagging vibration of these complexes is assigned to the bands observed at 696 (686), 695 (698) and 699

(707) cm^{-1}, respectively. The corresponding vibration of glycine is assigned to the band at 707 (697) cm^{-1}. The Cr–N stretching modes appear at 581 (578), 576 (577) and 515 (552) cm^{-1}, and the Cr–O bands appear at 468 (470), 469 (475) and 416 (415) cm^{-1}, respectively. Guindy et al. [14] reported Cr–O stretching bands in the 600 cm^{-1} region for chromium(III) coordinated to DL-leucine but they did not report a value for the Cr−N stretching band. The X-ray crystal structure of the facial tris(glycinate)chromium(III) complex has been reported by Bryan et al. [19], showing that the Cr–N and Cr–O bond distances are 2.068 and 1.965 Å, respectively, suggesting the Cr−N bond is weaker than the Cr−O bond and should have a higher frequency vibration. Robert et al. [47] measured the IR spectra of bis(glycine) complexes of Pt(II), Pd(II), Cu(II), and Ni(II) species, finding that the metal–nitrogen stretching bands (550–430 cm^{-1}) appear at higher frequencies than the metal–oxygen stretching bands (420–290 cm^{-1}), which is consistent with our systems. However, the effects of the molecular symmetry and H-bonding may also impact the $-NH_2$ and $-COO^-$ modes [48−49]. Nevertheless, the IR stretching bands of the tris-, bis- and mono-glycinatochromium(III) complexes in this study are in good agreement with theoretical values, which were obtained without explicit outer sphere solvation of the complexes (Table ST2 and Figs. S4−S13 of the SI).

3.3. DFT Studies of glycinato-chromium(III) complexes

The experimental characterization reveals that the tris-glycinatochromium(III) complex is quite stable in both solution and solid forms. In comparison, the TGA results imply that the mono-glycinatochromium(III) complex is the least stable and therefore likely to be the most reactive. Therefore we have investigated the mechanisms for aquation of these complexes.

3.3.1. Aquation mechanisms for open-type chromium(III) systems

Under acidic conditions, the mono-glycinatochromium(III) complex, $[Cr(H_2O)_4(gly)]^{2+}$ is expected to convert to $[Cr(H_2O)_5(^+NH_3CH_2COO^-)]^{3+}$ via a Cr–N ring opening with the two structures in equilibrium (see Figs. 3–4). This is supported by the observation of higher frequency vibrations for the Cr–N bonds compared with Cr–O bonds. In fact the Cr–N vibration of the tris complex has the highest frequency value in the series, suggesting it has the weakest Cr–N bond(s) and therefore will be most susceptible to ring-opening. Water exerts a weaker *trans* effect than carboxylate and hence there is an increase in the Cr–N bond strengths with aquation. All our attempts to locate a transition state for this ring opening process failed across the three bidentate systems. Therefore, we use the open-type structures ($[Cr(H_2O)_5(^+NH_3CH_2COO^-)]^{3+}$) as the starting point for investigation of aquation reactions. The structures of the reactants, transition states and products involved in the interchange mechanism of the aquation of $[Cr(^+NH_3CH_2COO^-)(H_2O)_5]^{3+}$ are presented in Scheme 1 and Figs. S14 to S16 of the SI.

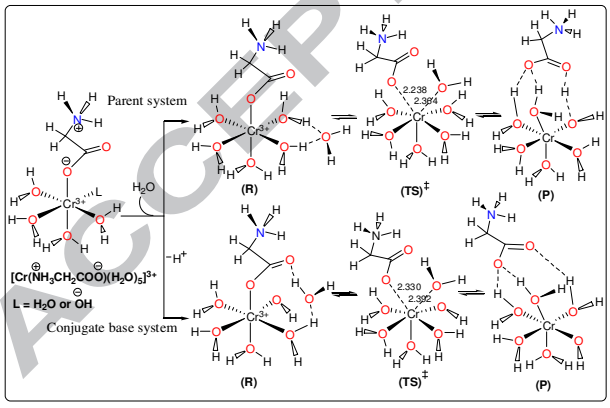

Scheme 1. Associative Interchange (I_a) mechanism for the aquation of $[Cr(^+NH_3CH_2COO^-)(H_2O)_5]^{3+}$ and $[Cr(^+NH_3CH_2COO^-)(H_2O)_4(OH)]^{2+}$ with H_2O.

As shown in Scheme 1, deprotonation of an inner sphere water molecule can also occur to give the conjugate base ($[Cr(^{+}NH_3CH_2COO^{-})(H_2O)_4(OH)]^{2+}$), which can subsequently undergo aquation in a similar manner to the parent complex (Figs. S17 to S20). Aquation reactions of $[Cr(^{+}NH_3CH_2COO^{-})(H_2O)_5]^{3+}$ can potentially occur via several different mechanisms including interchange and dissociative pathways.

The interchange pathway for aquation of both $[Cr(^{+}NH_3CH_2COO^{-})(H_2O)_5]^{3+}$ and $[Cr(^{+}NH_3CH_2COO^{-})(H_2O)_4(OH)]^{2+}$ is initiated by outer sphere coordination of a water molecule to the Cr(III)-glycinate species as shown in Scheme 1 (Figs. S14 to S20 of the SI). For both the neutral and conjugate base complexes, the incoming H_2O forms a hydrogen bond with an inner sphere water molecule, to give the stabilized precursor/reactant complex (R). The precursor structures (R) with outer-sphere coordination of the attacking nucleophilic water molecule involve bifurcated H-bonding to an inner sphere water molecule ($H_2O_{(inner)}$). Previously [27–29], we found that the precursor haloaqua Cr(III) structures with bifurcated bridging hydrogen bonds are energetically more stable than those with linear hydrogen bonds. IRC analysis of the transition states also confirms the bifurcated H-bonded structures (Scheme 1) as the precursors for aquation of both of $[Cr(^{+}NH_3CH_2COO^{-})(H_2O)_5]^{3+}$ and $[Cr(^{+}NH_3CH_2COO^{-})(H_2O)_4(OH)]^{2+}$ along the interchange pathway (Figs. S14 to S20). For these precursor species the bifurcated HO–H**…**O distances for H-bonding of $Cr–H_2O_{inner}$ with the outer sphere H_2O molecule are 1.61 and 1.63 Å for the parent system (Fig. S14) and 1.45 and 1.71 Å for the conjugate base system (Fig. S17 of the SI). These variations reflect differences in the electronegativity and distortion of geometry of these species.

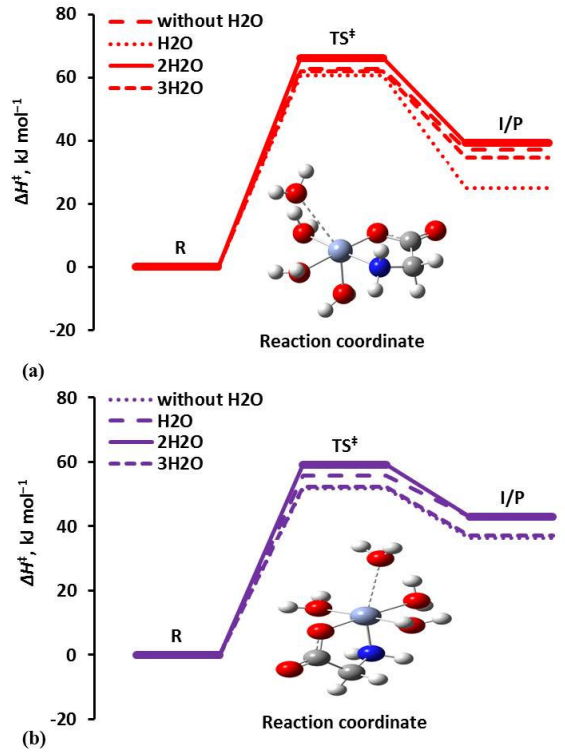

Fig. 8. Energy profiles (kJ mol^{-1}) for aquation via the interchange pathway of (a) $[Cr(^{+}NH_3CH_2COO^{-})(H_2O)_5]^{3+}$ and (b) $[Cr(^{+}NH_3CH_2COO^{-})(H_2O)_4(OH)]^{2+}$ with nH_2O (n =1–3) in solution phase obtained at PBE0/cc-pVDZ.

The energy profiles for aquation of $[Cr(^{+}NH_3CH_2COO^{-})(H_2O)_5]^{3+}$ and $[Cr(^{+}NH_3CH_2COO^{-})(H_2O)_4(OH)]^{2+}$ are shown in Figs. 8a•8b and the enthalpies of activation ($H^{\ddagger}$), Gibbs energies of activation ($G^{\ddagger}$) and entropies of activation ($S^{\ddagger}$) are given in Table 1.

Table 1
Enthalpies ($\Delta H^{\ddagger}$, kJ mol^{-1}), gibbs energies ($\Delta G^{\ddagger}$, kJ mol^{-1}), and entropies ($\Delta S^{\ddagger}$, J $mol^{-1}K^{-1}$) of activation for interchange pathways of $[Cr(H_2O)_5(^{+}NH_3CH_2COO^{-})]^{3+}$ and $[Cr(H_2O)_4(OH)(^{+}NH_3CH_2COO^{-})]^{2+}$ with H_2O in the solution phase at 298.15 K.[a]

	$[Cr(H_2O)_5(glyH)]^{3+}$			$[Cr(H_2O)_4(OH)(glyH)]^{2+}$		
nH_2O	$\Delta H^{\ddagger}$	$\Delta G^{\ddagger}$	$\Delta S^{\ddagger}$	$\Delta H^{\ddagger}$	$\Delta G^{\ddagger}$	$\Delta S^{\ddagger}$
1	114	128	–46	97	109	–42
2	110	113	–11	91	95	–14
3	88	102	–47	76	86	–35

[a] Optimized structures defined in Figs. S14 to S20 of the SI.

The aquation barrier for the conjugate base system is lower due to changes in the electronic environment and distortion of the complex geometry in the TSs (Table 1 and Figs. 8a–8b and 9). For example, the conjugate base system is less strained with a COO-**…**Cr**…**OH angle of 80.6° compared with a COO-**…**Cr**…**OH_2 angle of 69.7° in the parent complex. Likewise, the Cr–$O_{(inner)}$ bond lengths are 2.01 and 1.82 Å for the parent and conjugate base systems, respectively. In comparison, the transition Cr**…**OOC distances are very similar in both systems, (2.35 Å and 2.39 Å) (Figs. S14 to S20 of the SI). Likewise, the Cr(III)**…**OH_2 distances in the neutral and conjugate base are 2.36 Å and 2.39 Å, respectively.

In our previous study [29] of *cis*-$[Cr(H_2O)_4(OH)Cl]^+$ we found explicit outer-sphere water molecules are required to stabilise the transition states. Therefore, we also investigated the effects of inclusion of additional outer sphere water molecules on the aquation of $[Cr(H_2O)_5(^+NH_3CH_2COO^-)]^{3+}$ and it conjugate base species, via the interchange pathway (Figs. S14–S20 of the SI). In this work, three outer sphere water molecules were also found to be necessary to lower $\Delta H^{\ddagger}$ (Table 2 and Figs. S14–S20 of the SI). Hydrogen bonding between the departing glycinate ligand and the neighbouring water molecules assists the ligand transfer in these systems (Fig. 9). This is clearly demonstrated by the changes in activation enthalpies for the interchange pathway of $[Cr(H_2O)_5(^+NH_3CH_2COO^-)]^{3+}$**…**$3H_2O$ and its conjugate base complexes (88 and 76 kJ mol^{-1}, which are in good agreement with experimental [12] results (87 and 75 kJ mol^{-1}). The hydrogen bonding network around these complexes with three water molecules makes a relatively significant contribution to $\Delta H^{\ddagger}$, as shown by the decreases in the activation enthalpies (26 and 21 kJ mol^{-1}, respectively), compared to the corresponding one water systems (Figs. S14–S20 of the SI). The Cr**…**$^-OOCH_2{}^+NH_3$ distances in the TSs of

$[Cr(H_2O)_5(^+NH_3CH_2COO^-)]^{3+}$**…**$3H_2O$ complex and its conjugate base species are slightly longer than in the single H_2O systems (0.03 Å and 0.14 Å, respectively). The oxygen atom of the incoming water molecule and glycinate ion of the leaving group exhibits relatively little change in charge across the one, two and three water systems as shown in the selected maps of electrostatic potential (Fig. 9) for the interchange mechanism. We have determined the changes in $(\Delta\sum d(Cr{-}L)_{TS-R})$ are −0.71 Å and −0.65 Å for $[Cr(H_2O)_5(^+NH_3CH_2COO^-)]^{3+}$ and it conjugate base species with H_2O, which corresponds with a negative activation volume ($\Delta V^{\ddagger}$) associated with an I_a mechanism, and is consistent with experimental results [12].

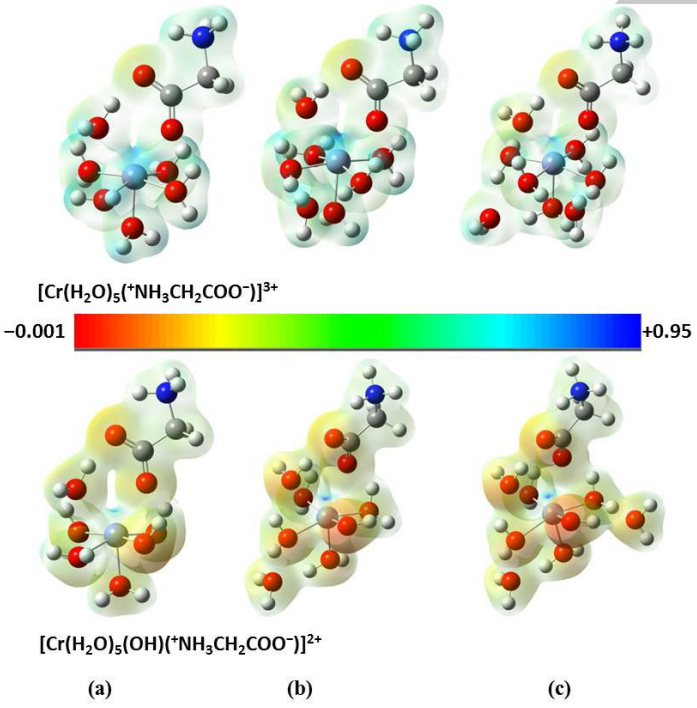

Fig. 9. Optimized transition structures of $[Cr(H_2O)_5(^+NH_3CH_2COO^-)]^{3+}$ and $[Cr(H_2O)_4(OH)(^+NH_3CH_2COO^-)]^{2+}$ for (a) H_2O, (b) $2H_2O$, and (c) $3H_2O$ via interchange pathway and maps of electrostatic potential (0.02 electrons $Bohr^{-3}$) (red = electron-rich, blue = electron-deficient).

For comparison, we have also investigated the dissociative (*D*) mechanism, which involves breaking the Cr(III)–$^{-}$OOCH$_2$$^{+}NH_3$ bond with formation of a pentaqau- or tetraaquahydroxo-coordinated intermediate (Scheme 2). The released $^{-}$OOCH$_2$$^{+}NH_3$ ion is coordinated to the outer sphere of the intermediate complexes (I) to give an ion-pair as shown in Figs. S21 to S22 of the SI.

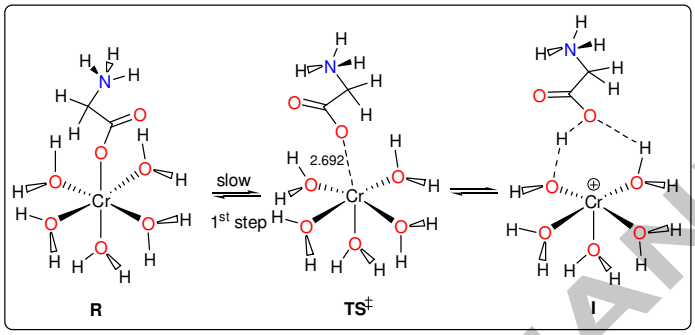

Scheme 2. Dissociative (*D*) mechanism for the reaction of [Cr($^{+}$NH$_3$CH$_2$COO^{-})(H$_2$O)$_5$]$^{3+}$.

The enthalpy of activation, Gibbs energy of activation and entropy of activation for Cr(III)-$^{-}$OOCH$_2$$^{+}NH_3$ bond dissociation of [Cr($^{+}$NH$_3$CH$_2$COO^{-})(H$_2$O)$_5$]$^{3+}$ are 138 kJ mol^{-1}, 144 kJ mol^{-1} and –22 J mol^{-1} K^{-1}, respectively (see Table ST3 and Figs. S21–S22 of the SI), indicating that this pathway is energetically less favourable than the interchange pathway. However, we have previously [28–29] shown an improved model of the dissociation process is achieved when water is coordinated to the outer sphere of the complex, which also lowers $\Delta H^{\ddagger}$ for the dissociation step (Table ST3 of the SI (Figs. S21–22 of the SI). The $\Delta H^{\ddagger}$ values for the Cr–OglyH dissociation of the precursor complex with an explicit outer sphere water molecule is lower (Fig. S22) by 5 kJ mol^{-1} compared to bond dissociation without the outer sphere water molecule (Fig. S21). Nevertheless, the activation energy for this pathway remains substantially higher than for the interchange pathway discussed earlier. The Cr**…**OglyH distances in the TS,

without and with the outer-sphere water molecule are quite similar (2.69 Å to 2.66 Å, respectively) (Figs. SF21 to SF22 of the SI), reflecting the relatively small contribution the additional H-bonding makes to this process.

In our previous work [30], we found that the UV-Vis spectrum of *fac*-[Cr(gly)$_3$] in the solid state showed peaks at 510 nm (v_1) and 388 nm (v_2), whereas in DMSO the two spin-allowed peaks were shifted to longer wavelengths (518 nm and 393 nm, respectively). Bryan et al. [19] assigned the spin allowed d-d transition at 503 nm to $^4A_{2g} \rightarrow {}^4T_{2g}$ (v_1) and 384 nm to $^4A_{2g} \rightarrow {}^4T_{1g}$ (v_2). As noted here, the aqueous solution UV-Vis spectrum shows bands at 527 nm (44.2 M^{-1} cm^{-1}) and 395 nm (23.6 M^{-1} cm^{-1}) and the pH of the solution is 6.02. One explanation for this is that in acidic aqueous solution, the tris complex undergoes Cr–N ring opening via an acid catalysed aquation pathway with coordination of a water molecule, and that this structure is in equilibrium with the closed structure. Protonation of the glycine ligands may occur via intramolecular hydrogen transfer to form the conjugate base.

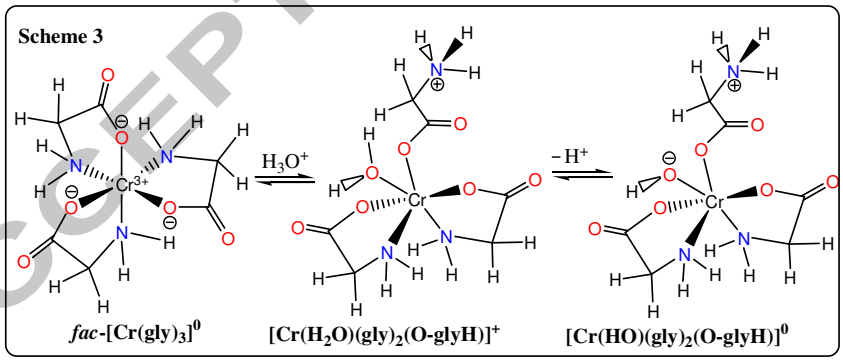

Aquation of the [Cr(H$_2$O)(gly)$_2$(O–glyH) complex occurs via a two-step process. Firstly, direct Cr…O-glyH bond breaking and formation of an intermediate as shown in Scheme 3 (see Figs. S23–S24). Secondly, this intermediate can easily add H$_2$O to form the corresponding product as

shown in Scheme 4. The $\Delta H^{\ddagger}$ value for dissociation of the Cr–gly bond for this pathway is 97 kJ mol^{-1} (Scheme 4 and Fig. S23 of the SI), with the amines being *cis* and the COO^- groups having *trans* configuration. Furthermore, the overall activation enthalpy is 97 kJ mol^{-1}, which is in good agreement with the experimental[23] value (91.4 ± 2 kJ mol^{-1}) (Table ST4 and Fig. S24).

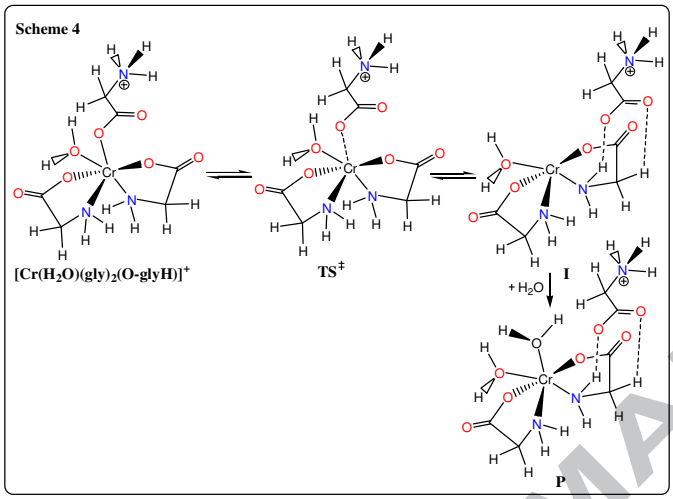

The aquated complexes can also undergo reaction via replacement of the aqua ligands. Therefore, we investigated Cr–OH_2 dissociation for *cis* and *trans*-$[Cr(H_2O)_4(gly)]^{2+}$ with up to three explicit outer sphere water molecules ($[Cr(H_2O)_4(gly)]^{2+}$**…***n*H_2O, *n* = 0 to 3) (Table 2 and Figs. S25 to S33 of the SI). Dissociation of the Cr–OH_2 bond (63 kJ mol^{-1}) is a much lower energy process than dissociation of the Cr-OglyH bond (138 kJ mol^{-1}). Overall, the addition of explicit outer-sphere water molecules has a relatively small effect on the activation enthalpy for this process. However, there is a noticeable difference in the activation parameters for the two isomers. For example, the dissociation of the Cr–OH_2 bond (TS) (Fig. 10a–10b) for cis-$[Cr(H_2O)_4(gly)]^{2+}$**…**$3H_2O$ has $\Delta H^{\ddagger}$ = 62 kJ mol^{-1}, whereas for the *trans* complex $\Delta H^{\ddagger}$ = 52 kJ mol^{-1} (Table 2 and Fig. 10). No interchange pathway was identified for water-water exchange on this complex.

Table 2
Enthalpies ($\Delta H^{\ddagger}$, kJ mol^{-1}), gibbs energies ($\Delta G^{\ddagger}$, kJ mol^{-1}), and entropies ($\Delta S^{\ddagger}$, J mol^{-1}K^{-1}) of activation for dissociation pathway of $[Cr(H_2O)_4(gly)]^{2+}$ with $n$$H_2O$ in the solution phase at 298.15 K.[a]

	***cis*-$[Cr(H_2O)_4(gly)])]^{2+}$**			***trans*-$[Cr(H_2O)_4(gly)])]^{2+}$**		
$n$$H_2O$	$\Delta H^{\ddagger}$	$\Delta G^{\ddagger}$	$\Delta S^{\ddagger}$	$\Delta H^{\ddagger}$	$\Delta G^{\ddagger}$	$\Delta S^{\ddagger}$
0	63	67	–16	52	60	–26
1	61	63	4	56	61	–16
2	66	71	–15	59	60	–3
3	62	63	–3	52	55	–8

[a] Optimized structures defined in Figs. S25–S33 of the SI.

The structures for the corresponding dissociation of $[Cr(OH)(H_2O)_3(gly)]^{+}$ are shown in Figs. S34 to S39 of the SI. The $\Delta H^{\ddagger}$ values for the Cr–OH_2 dissociation in the $[Cr(OH)(H_2O)_3(gly)]^{+}$…$n$$H_2O$ (n = 0–2) complexes are lower than for the parent species by 7 to 11 kJ mol^{-1} (Table ST5 of the SI). In both systems, the values for Cr…OH_2 dissociation from the *trans* position are 9 to 12 kJ mol^{-1} lower than the corresponding values for the *cis*-systems (Table ST5 and Figs. S34–S39).

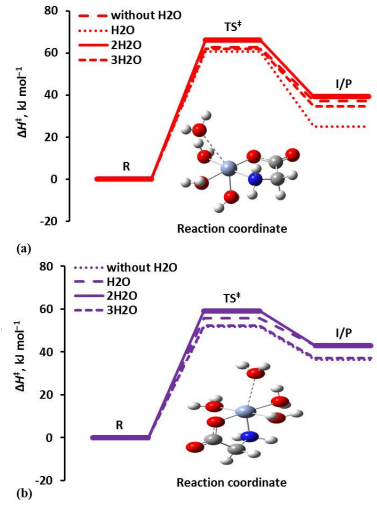

Fig. 10. Energy profiles (kJ mol^{-1}) for the dissociation pathway of (a) *cis* and (b) *trans* position dissociation of $[Cr(H_2O)_4(gly)]^{2+}$…$n$$H_2O$ (n =0–3) in solution phase obtained at PBE0/cc-pVDZ.

The bis-glycinatochromium(III) complex can also undergo reaction via release of an inner-sphere water molecule. The transition structures for the Cr(III)…OH_2^+ bond dissociation step of *cis*-[Cr($^+NH_3CH_2COO^-$)$_2$(H_2O)$_2$]$^+$ (A and B) (Figs. S40–S42 of the SI), and *trans*-[Cr($^+NH_3CH_2COO^-$)$_2$(H_2O)$_2$]$^+$ (C) (Figs. S43–S45) are shown in Fig. 11. The enthalpies of activation for these different conformations are 57, 62 and 80 kJ mol^{-1}, respectively (Table ST6 of the SI). The oxygen atom of the departing water molecule is more negatively charged in the TS of the *trans*-system (–0.962) than in either of the *cis*-TS structures investigated (–0.920 and –0.926), which suggests a trans-effect in these complexes in the order H_2O < NH_2R < ^-O_2CR. (Fig. 11). Furthermore, NBO [33] charge analysis of the TSs shows an increase in the positive charge on Cr(III) compared to R as shown in Fig. S46 of the SI. The $\Delta H^{\ddagger}$ values for the corresponding conjugate base systems are 54, 52 and 41 kJ mol^{-1} (Table ST7), respectively, due to changes in the electronic environment and the *trans*-effect of OH^- in system C (see Figs. S47–S49 of the SI).

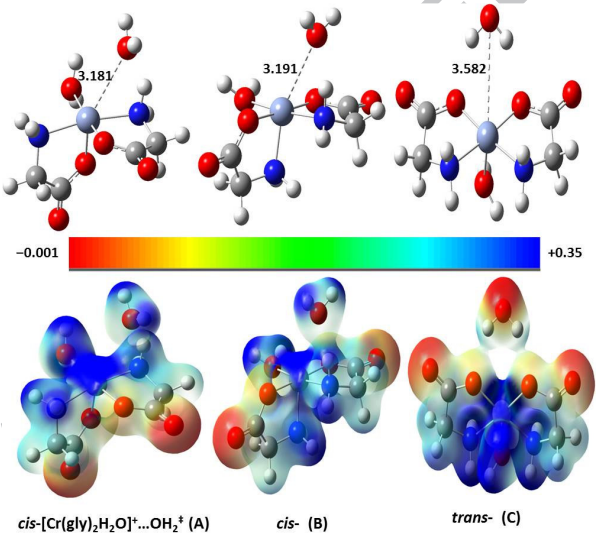

Fig. 11. Structures of *cis* (A–B) and *trans* (C) position dissociation of [Cr(H_2O)(gly)$_2$]$^+$ …H_2O and maps of electrostatic potential (0.02 electrons Bohr^{-3}) (red = electron-rich, blue = electron-deficient).

3.5. Discussion

In this study, we have carried out a detailed investigation of the associative interchange (I_a) and dissociation (D) mechanisms for the aquation of mono- and tris-(glycinato) chromium(III) complexes. The activation enthalpies for aquation of $[Cr(H_2O)_5(NH_3^+CH_2COO^-)]^{3+}$ and its conjugate base were found to be 88 and 76 kJ mol^{-1} respectively, via the I_a pathway with inclusion of explicit outer sphere solvation ($3H_2O$), which is in good agreement with experimental [12] results (87 and 75 kJ mol^{-1}). Outer-sphere solvation makes a significant contribution to $\Delta H^{\ddagger}$, as shown by the decreases in the activation enthalpies (26 and 21 kJ mol^{-1}, respectively), compared to the corresponding one water systems. Significantly, higher enthalpies of activation were obtained via the dissociative pathway for the mono-glycinatochromium(III) complex (138 kJ mol^{-1} and 144 kJ mol^{-1}, respectively). However, for the sterically crowded $[Cr(gly)_3]$ complex, the dissociative mechanism was identified as the preferred aquation pathway.

A key feature of the UV-Vis experimental investigation of the mono-, bis- and tris-glycinatochromium(III) bidentate complexes is the effect of pH. In the highly acidic environment of the stomach (pH = 3–4), orally ingested nutritional supplements will likely undergo slow aquation, leading to a mixture of mono-, bis- and tris-glycinatochromium(III) complexes. However, when these complexes enter the duodenum they will encounter an environment with a much milder pH, the mono-glycinatochromium(III) complex is expected to undergo rapid deprotonation to form the corresponding conjugate base species.

4. Conclusions

We have prepared mono-, bis- and tris-glycinatochroium(III) species and characterized them by thermogravimetry, UV-Vis (in the range pH of ~3.0 to ~8.5), EPR (both solid and frozen states), ATR-FTIR and Raman spectroscopy. Vibrational frequencies calculated at PBE0/cc-pVDZ are in good agreement with experimental values. The TGA-DSC analysis indicates a progressive structural change along the decomposition reaction, with major endothermic transitions found at 370, 390, and 424.0 °C [30] for mono-, bis- and tris-glycinatochromium(III) species, respectively. Geometries (bond lengths and bond angles) at PBE0/cc-pVDZ are in good agreement with the X-ray crystal data of *fac*-[Cr(gly)$_3$] [19]. Aquation of the mono-glycinatochromium(III) complex is found to follow the associative interchange (I_a) pathway for the ring-opened isomer with $\Delta H^{\ddagger}$ values in good agreement with the experimental data [12], for both parent and conjugate base forms of the complex. In comparison, tris-glycinatochromium(III) undergoes aquation via the dissociative (D) pathways. These results may provide further insight into whether or not these complexes can either undergo binding to proteins or can form oligomers in biological systems.

Acknowledgements

We thank to Professor Bogdan Dlugogorski for providing access to the EPR and TGA-DSC facilities. In addition, we are grateful to the Australian National Computational Infrastructure (NCI) facility and the Atlantic Computational Excellence Network (ACENET) for computer time.

Supplementary material

Supplementary data associated with this article can be found, in the online version.

References

[1] W. Mertz, Physiol. Rev. 49 (1969).
[2] W. Mertz, *Nutr. Rev.* 33 (1975) 129.
[3] C. L. Rollinson, In Problems of chromium reactions, Andrews Radioactive Pharmaceuticals US Atomic Energy Commission Conference, 1966; p 429.
[4] C. Rollinson, E. Rosenbloom, J. Lindsay, Proc. VII Intern. Congr. Nutr 5 (1967).
[5] H. A. Schroeder, Am. J. Clin. Nutr. 21 (1968) 230.
[6] K. Schwarz, W. Mertz, Arch. Biochem. Biophys. 85 (1959) 292.
[7] J. Vincent, The nutritional biochemistry of chromium (III). Elsevier: 2011.
[8] J. B. Vincent, Proc Nutr Soc 63 (2004) 41.
[9] H.-y.Tang, Q.-g. Xiao, H.-b. Xu, Y. Zhang, Org. Process Res. Dev. 17 (2013) 632.
[10] H.-y. Tang, Q.-g. Xiao, H.-b. Xu, Y. Zhang, J. Trace Elem. Med Biol. 29 (2015) 136.
[11] I. A. Khan, J. Inorg. Nucl. Chem. 43 (1981) 1082.
[12] M. Abdullah, J. Barrett, P. O'Brien, J. Chem. Soc., Dalton Trans. 8 (1984) 1647.
[13] T. Ramasami, R. Taylor, A. Sykes, Inorg. Chem. 15 (1976) 2318.
[14] N. Guindy, Z. Abou-Gamra, M. Abdel-Messih, J. Chim. Phys. Phys.- Chim. Biol. 96 (1999) 851.
[15] N. M. Guindy, Z. M. Abou-Gamra, M. F. Abdel-Messih, *Monatsh. Chem.* 131 (2000) 857.
[16] D. Banerjea, S. D. Chaudhuri, J. Inorg. Nucl. Chem. 30 (1968) 871.
[17] I. A. Khan, Int. J. Chem. Kinet. 17 (1985) 1263.
[18] T. Ramasami, R. K. Wharton,A. G. Sykes, Inorg. Chem. 14 (1975) 359.
[19] R. F. Bryan, P. T. Greene, P. F. Stokely, E. W. Wilson Jr, Inorg. Chem. 10 (1971) 1468.
[20] H. Ley, K.Ficken, Ber. Dtsch. Chem. Ges. 45 (1912) 377.
[21] A. Earnshaw, J. Lewis, , J. Chem. Soc. (1961) 396.
[22] J. T. Veal, W. E. Hatfield, D. Y. Jeter, J. C. Hempel, D. J. Hodgson, Inorg. Chem. 12 (1973) 342.
[23] E. Kita, H. Marai, T. Muzioł,K. Lenart, Transit Metal Chem 36 (2011) 35.
[24] E. Kita, R. Lisiak, Transit Metal Chem 36 (2011) 855.
[25] E. Kiersikowska, H. Marai,; M. Mątewska, G. Wrzeszcz, E. Kita, Transit Metal Chem 39 (2014) 361.
[26] E. Kita, E. Kiersikowska, H. Marai, Transit Metal Chem 39 (2014) 63.
[27] K. M. Uddin, D. Ralph, D. J. Henry, Comp. Theor. Chem. 1070 (2015) 152.
[28] K. M. Uddin, R. A. Poirier, D. J. Henry, Comp. Theor. Chem. 1084 (2016) 88.
[29] K. M. Uddin, D. J. Henry, ChemistrySelect 1 (2016) 5236.
[30] K. M. Uddin, A. M. Habib, D. J. Henry, ChemistrySelect 2 (2017) 1950.
[31] M. Frisch, G. Trucks, H. B. Schlegel, G. Scuseria, M. Robb, J. Cheeseman, G. Scalmani,V. Barone, B.Mennucci, G. Petersson, Gaussian 09, Revision A. 02, Gaussian. Inc., Wallingford, CT 200, 2009.
[32] S. Miertuš, E. Scrocco, J. Tomasi, Chem. Phys. 55 (1981) 117.
[33] J. Tomasi, B. Mennucci, R. Cammi, Chem. Rev. 105 (2005) 2999.
[34] A. E. Reed, L. A. Curtiss, Chem. Rev. 88 (1988) 899.
[35] K. Emerson, W. Graven, J. Inorg. Nucl. Chem. 11 (1959) 309.
[36] N. Bjerrum, Z. phys. Chem 59 (1907) 336.
[37] P. J. Elving, B. Zemel, J. Am. Chem. Soc. 79 (1957) 1281.

[38] J. A. Cooper, L. F. Blackwell, P. D. Buckley, Inorg. Chim. Acta 92 (1984) 23.
[39] S. Shuttleworth, R. Sykes, J. Am. Leather Chem. Assoc. 54 (1959) 259.
[40] A. R. Freitas, M. Silva, M. L. Ramos, L. L. Justino, S. M. Fonseca, M. M. Barsan, C. M. A. Brett, M. R. Silva, H. D. Burrows, Dalton Trans. 44 (2015)11491.
[41] B. M. Weckhuysen,R. A. Schoonheydt, F. E. Mabbs D. Collison, J. Chem. Soc., Faraday Trans. 92 (1966) 2431.
[42] B. M. Weckhuysen, L. M. De Ridder, P. J. Grobet, R. A. Schoonheydt, J. Phys. Chem. 99 (1995) 320.
[43] W. T. M. Andriessen, M. P. Groenewege, Inorg. Chem. 15 (1976) 621.
[44] D. N. Sen, S. Mizushima, C. Curran, J. V. Quagliano, J. Am. Chem. Soc. 77 (1955) 211.
[45] C. Mateescu, C. Gabriel, C. P.Raptopoulou, A.Terzis, V.Tangoulis,A. Salifoglou, Polyhedron 52 (2013) 598.
[46] K. Nakamoto, Infrared and raman spectra of inorganic and coordination compounds, 5th ed., J. Wiley, New York, 1997.
[47] R. A. Condrate,; K. Nakamoto, J. Chem. Phys. 42 (1965) 2590.
[48] A. W. Herlinger,T. V. Long, J. Am. Chem. Soc. 92 (1970) 6481.
[49] A. W. Herlinger, S. L. Wenhold, T. V. Long, J. Am. Chem. Soc. 92 (1970) 6474.

Table of Contents (TOC):

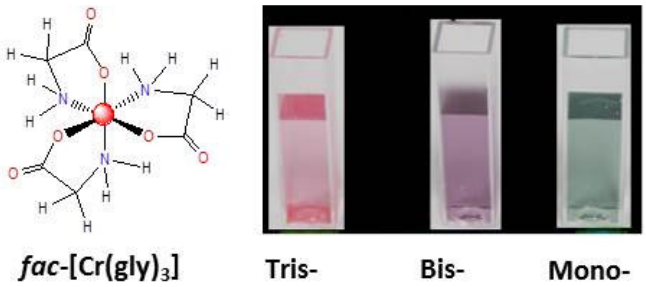

Synopsis: Mono-, bis- and tris-glycinatochromium(III) complexes were synthesized and fully characterized. The effects of pH on aquation were investigated experimentally by UV-Vis spectroscopy and theoretically by DFT calculations and provide insight to the physiological speciation of these complexes.